SAE Technical Paper Series. Automotive Technical Papers, Paper number 2025-01-5029
DOI:10.4271/2025-01-5029

On the application of trapped vortices in motorsport application for improved aerodynamic performance using passive and active flow control

Ming Kin NG* and Tom-Robin Teschner
Affiliation
(Dated: May 6, 2025)

New regulations introduced by the *Fédération Internationale de l'Automobile* (FIA) for the 2026 Formula 1 season mark the first instance of active flow control methods being endorsed in Formula 1 competition. While active methods have demonstrated significant success in airfoil development, their broader application to grounded vehicle aerodynamics remains unexplored. This research investigates the effectiveness of Trapped Vortex Cavity (TVC) technology in both active and passive flow control, applied to a NACA0012 airfoil and an inverted three-element airfoil from a Formula 1 model. The investigation is conducted using numerical methods to evaluate the aerodynamic performance and potential of TVC in this paper. In the single airfoil case, a circular cavity is placed along the trailing edge (TE) on the suction surface; for the three-element airfoils, the cavity is positioned on each airfoil to determine the optimum location. The results show that the presence of a cavity, particularly with active flow control, significantly improves the lift-to-drag ratio (C_L/C_D) for both the single airfoil and the three-element airfoils. A maximum enhancement of 1160% was recorded for the single airfoil, while the three-element airfoils saw an improvement of 313% compared to their original configurations. However, when the TVC was placed in positions other than the trailing edge of the mid airfoil, a performance reduction was observed, even with active blowing applied. The passive flow control approach, which requires no additional energy input, yielded a modest improvement of 3.52% for the NACA0012 airfoil. However, passive control underperformed due to unstable vortex interactions with each airfoil element for the inverted three-element airfoil case. Even with optimal placement and geometrical modifications, the maximum C_L/C_D ratio for passive control was only 96% of the original C_L/C_D of the unmodified three-element airfoils, suggesting that passive flow control is less effective here compared to active flow control.

Keywords: Trapped vortices, Active flow control, Passive flow control, Aerodynamics performance

I. INTRODUCTION

To ensure competitiveness in Formula 1, new regulations have been introduced by the Fédération Internationale de l'Automobile (FIA) for the 2026 season. In contrast to previous rules that strictly prohibited active flow control, the latest regulations permit the use of active aerodynamic systems on the front wing. These systems allow drivers to switch different aerodynamic modes to optimize performance based on real-time racing conditions. This shift in FIA's stance opens up new opportunities for implementing active aerodynamics, mainly through techniques such as blowing and suction, which involve the injection of energy into the airflow to enhance performance [1].

Active flow control offers significant advantages in delaying flow separation and increasing the suction effect, thereby helping to maintain an optimal lift-to-drag ratio (C_L/C_D). A well-balanced C_L/C_D ratio is critical for racing performance, especially on demanding circuits like the Monaco Grand Prix, where aerodynamic efficiency plays a crucial role in cornering stability. A higher C_L/C_D ratio in high-speed corners like Tabac can enhance traction, allowing closer racing distances and creating more overtaking opportunities on the following straight. A generic race car can achieve a lap time improvement of up to 62 seconds if it operates at its optimal performance, maximizing the C_L/C_D. Specifically, an increase in aerodynamic downforce, with increasing from 0 to -2.0, significantly enhances aerodynamic efficiency. This improved efficiency enables the vehicle to gain a competitive advantage by achieving better positioning in a race [2]. Given the importance of maintaining an optimal C_L/C_D ratio in these conditions, this paper investigates the application of active aerodynamic systems on the front wing of a Formula 1 car, with a particular focus on how these systems can enhance racing performance through improved aerodynamic efficiency.

The front wing of a Formula 1 model, in contrast to aircraft wings, is designed as an inverted airfoil that operates closely to the ground. Due to its proximity to the ground, an interaction between the airflow and the ground is induced, commonly referred to as the ground effect, causing the constrained airflow on the suction surface to accelerate. This acceleration, combined with the camber of the wing, reduces the pressure underneath, and therefore, downforce is generated.

* Correspondence email address: mingkin.ng@cranfield.ac.uk

The front wing consists of three main elements that work together to optimize aerodynamic performance. The slat at the front helps extend the angle of attack, and delays flow separation by maintaining airflow attachment. The midsection accelerates airflow toward the flap due to its negative camber, while the flap, with its high angle, induces greater circulation around the main element, resulting in increased suction on the lower surface and higher pressure on the upper surface, which enhances overall downforce.

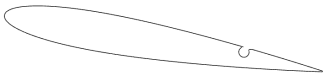

Figure 1: TVC concept applied in NACA0012: Upper side is suction surface and bottom side is pressure surface

To further enhance the aerodynamic performance of the front wing, the Trapped Vortex Cavity (TVC) concept is introduced in this paper as a potential method to maximize the C_L/C_D. The TVC is based on a vortex which is anchored inside a cavity placed near the flow separation region along the suction surface of an airfoil, as displayed in Figure 1. By trapping a stable vortex within the cavity, the recirculating flow is encouraged to reattach to the surrounding airflow, thereby delaying flow separation. Through this mechanism, aerodynamic efficiency can be significantly improved by reducing drag and maintaining lift. Although the TVC has received some attention within the aeronautical research community, it has yet to be explored for motorsport applications, particularly in the context of inverted airfoils used on Formula 1 front wings. Therefore, its implementation in motorsport is considered a promising, untapped opportunity for performance gains.

This paper focuses on implementing active and passive aerodynamic methods within the TVC based on numerical investigation.First, a thorough literature review will be conducted to understand the development of TVC in the airfoil domain, including its current benefits and limitations. Then, the study's simulation result will be performed. A single airfoil will be used to demonstrate the concept and validate the approach. Following that, the TVC will be integrated into the three elements airfoils from a Formula 1 car to analyze and optimize the C_L/C_D ratio. The goal is to determine the most effective configuration for maximizing performance under racing conditions.

II. LITERATURE REVIEW

The concept of generating vortices has been widely implemented in motorsport to improve the aerodynamic efficiency of wings in racing cars. Several studies have investigated methods to enhance the lift-to-drag ratio (C_L/C_D) through passive flow control devices. Katz et al. [3, 4] explored the effectiveness of vortex generators on a flat plate, demonstrating that vortex generators successfully formed streamwise vortices. These vortices energized the boundary layer, suppressing flow separation and increasing downforce. Building on this work, Kuya et al. [5] advanced the research by placing vortex generators on the midsection of a race car wing. Their study showed that vortex generators, with a height equal to 20% of the boundary layer thickness, delayed flow separation from 65–80% to over 80% of the chord length. However, this improvement in downforce came at the cost of increased drag compared to a clean airfoil configuration.

In a parallel line of research, Basso et al. [6] applied Gurney flaps to the trailing edge of the wing's flap. The Gurney flaps, formed by extruded aluminum strips, generated a circulation pool by shifting the wake downward [7], resulting in a significant 24% increase in downforce. Unfortunately, this increase was accompanied by a 28% drag penalty, underscoring the inherent trade-off between lift and drag in such passive aerodynamic devices. While both vortex generators and Gurney flaps provided considerable performance improvements, they also introduced notable drag penalties. These methods rely on passive flow control techniques that suppress flow separation by geometrically modifying the wing, thereby applying their effects consistently across the flow regime [8]. A key limitation of these passive systems is their inability to dynamically adjust to changing racing conditions, which restricts their efficiency in optimizing the C_L/C_D.

In contrast to the methods mentioned above, the concept of Trapped Vortex Cavity (TVC) offers an

alternative flow control method by enlarging the suction effect generated by a trapped vortex anchored inside the cavity that is placed near the wake region on the suction surface of an airfoil. This design encourages reattachment of the flow, preventing flow separation and allowing for an increase in the angle of incidence, which helps to avoid stall conditions and improve aerodynamic efficiency without the same level of drag penalties. The trapped vortex concept was first proposed by Ringleb [9], and the Kasper wing, developed in 1974 [10], was one of the earliest applications based on this principle. The Kasper wing reportedly achieved an increase in lift coefficient at low Reynolds numbers.

However, experiments by Kruppa [11] revealed a significant issue with vortex shedding, which resulted in a substantial drag penalty rather than the anticipated lift enhancement. These findings underscored the need to trap the vortex inside the cavity and keep it in a nearly steady state to prevent vortex shedding. Similarly, wind tunnel experiments conducted by Donelli et al. [12] further concluded that anchoring the vortex within the cavity is challenging without an active control mechanism. To address this challenge, De Gregorio et al. [13] demonstrated that applying blowing slot inside the cavity can form a coherent vortex, thereby significantly reducing vortex shedding and enhancing overall aerodynamic performance.

Further CFD studies have reinforced these findings. De Gregorio et al. [13] compared an airfoil at a 7° angle of attack with and without a trapped vortex cavity, demonstrating that active TVC flow control can effectively manage flow separation and requires only a limited blowing coefficient. Similarly, Tutty et al. [14] emphasized that constant active flow is necessary to stabilize the flow within the cavity, which helps prevent large-scale vortex shedding. Lasagna et al. [15] investigated a NACA 0024 airfoil equipped with a trapped vortex cavity, showing that the introduction of blowing significantly improves drag reduction at low angles of incidence ($-2° < \alpha < 8°$) and a Reynolds number of approximately 10^6. This study revealed that, with blowing slot applied, the TVC system effectively delays flow separation. Panigrahi et al. [16] further explored the same airfoil configuration, concluding that a constant mass-flow rate (MFR) is sufficient to enhance the efficiency of the TVC airfoil, leading to an improved C_L/C_D ratio compared to a clean airfoil. Additionally, the stall angle was increased from 10° to 14° due to the application of active flow control.

The cavity shape in a TVC system is another important factor in improving the C_L/C_D performance of TVC-equipped airfoils. One notable example is the Vortex Cell 2050, which provides a platform for the design of vortex cells aimed at better incorporating trapped vortex and active flow control into thicker airfoils. Panigrahi et al. [16] introduced a third-order Bézier curve to optimize the shape of the cavity, demonstrating improved results for the optimized TVC shape compared to the non-optimized version. Vuddagiri et al. [17] compared various cavity shapes, including cavities inclined toward the downstream edge and upstream edge and elliptical, vertical, and circular cavities. The results suggested that the circular cavity performed better, as no secondary vortices were observed, whereas other shapes exhibited vortex breakdown.

The location of the TVC along the suction surface of an airfoil also plays a crucial role in affecting the C_L/C_D performance. Vuddagiri et al. [17] compared the performance of a circular cavity placed at the leading edge, mid-chord, and trailing edge, and the results suggested that the C_L/C_D ratio was highest when the cavity was located at the leading edge and trailing edge. Anand et al. [18] explained that positioning the TVC at the leading edge can cause flow acceleration over the frontal area, leading to an early transition to a turbulent boundary layer. This early transition makes the early reattachment hard to reconnect to the downstream of the cavity, causing a drag increment. As a result, placing the TVC beyond $x/c \approx 0.5$ is recommended for future studies.

It has been demonstrated that simply placing a TVC and treating it as a passive flow control method is ineffective at trapping the vortex within the cavity. However, the potential of other passive flow control techniques, particularly those involving geometrical modifications, has been recognized as a promising alternative. In a comparative experimental and computational study, Prince et al. [19] investigated the use of high pressure from the leading-edge stagnation point to feed air jets on the upper surface through a channel. This approach successfully delays flow separation and tolerates a higher angle of attack, thereby avoiding stall conditions without requiring an active system or incurring significant drag penalties.

The concept of a passive blowing channel has been identified as having potential when combined with the TVC. This channel could provide blowing power for stabilizing the vortex inside the cavity without additional energy input. This combination of passive techniques has been proposed as a promising solution for maintaining the coherence of the vortex within the cavity, potentially enhancing the aerodynamic performance of TVC-equipped airfoils.

III. METHODOLOGY

A. Geometry and Cavity design

This study investigates two primary geometries. The first geometry is a baseline NACA0012 airfoil with a chord length of 1 meter. The second geometry is a cross-sectional area (Figure 2) derived from the front wing of a 2022 baseline Formula 1 model, as shown in Figure 3 and Figure 4. The three-dimensional front wing is enclosed within a bounding box with dimensions of 0.9 m in length, 2 m in width, and 0.39 m in height. The cross-sectional profile of the wing comprises three elements: a slat, a mid airfoil, and a flap. The total chord length of the combined airfoil elements is 0.4325 m.

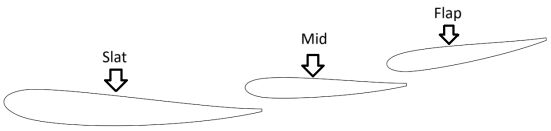

Figure 2: Cross-sectional area of the front wing; the first element airfoil is slat, second element airfoil is mid, third element is flap: Upper side is pressure surface and bottom side is suction surface

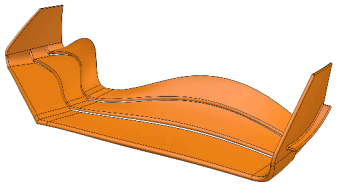

Figure 3: 3D model of the front wing used in the study

For the NACA0012 airfoil case, the study was conducted at an angle of incidence of 10 degrees with a Reynolds number of 6×10^6, facilitating comparison with the experimental results provided by Ladson [20]. The cavity on the airfoil is circular in shape and incorporates several critical flow features as seen in Figure 5, including the Cusp Point, where the flow changes direction and is redirected toward the stagnation region; the Stagnation Point, where the flow velocity becomes zero and the flow divides;

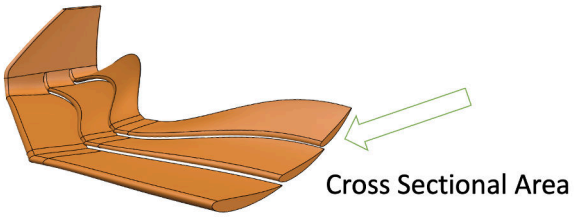

Figure 4: Cross sectional area being assessed in 2D case

and the Inflection Point, where the pressure gradient reverses. These key flow characteristics have been studied by Donelli et al. [12] and Vuddagiri et al. [17]. In this study, the Trapped Vortex Cavity (TVC) is located on the suction surface at approximately $x/c = 0.75$ (x/c = $TVC_{location}$/ Chord Length).

For the three-element airfoil cases, the study was conducted at a freestream Reynolds number of 1.5×10^6, corresponding to a velocity of 50 m/s. This Reynolds number, different from the NACA0012 case, was selected to reflect specific racing conditions, such as cornering, where aerodynamic performance—especially in C_L/C_D—is critical. The selection of 50 m/s is representative of high-speed corners on racetracks where overtaking opportunities exist, particularly in sections following a corner. For example, Suzuka's Turn 14 has an average speed of 175 km/h (48.6 m/s)[21], and the subsequent straight provides a prime overtaking opportunity. Similarly, in high-speed corners like Chapel at Silverstone (Turn 13), cars can reach speeds of 220 km/h (61.1 m/s)[22]. Therefore, the chosen velocity of 50 m/s represents the aerodynamic conditions in these overtaking zones, falling within a comparable velocity range.

The cavity structure applied to the three-element airfoils is similar to that of the NACA0012 airfoil. Several cavity locations were considered, including the leading edge, mid-chord, and trailing edge of the main airfoil, as well as the trailing edges of the slat and flap airfoils, with the primary objective of optimizing the TVC's location for enhanced aerodynamic performance.

Blowing flow was applied near the Cusp Point for both geometries as shown in Figure 5. The mass flow rate is given as

$$\dot{m}_{\text{in}} = V_{\text{in}} \rho A, \tag{1}$$

where V_{in} is the velocity entering the cavity at the blowing slot location, normal to the the boundary, ρ is the air density, and A is the cross-sectional area of the

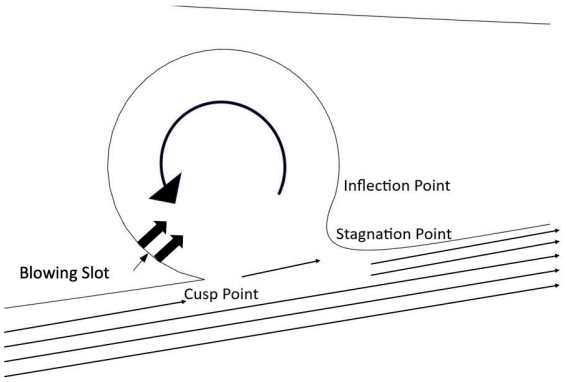

Figure 5: Features of the TVC

blowing slot.

For the passive aerodynamics cases, a blowing channel is introduced in both the NACA0012 airfoil and the inverted three-element airfoils. This channel links the stagnation point to the TVC. The performance of the channel is examined in terms of the length ratio between the tunnel inlet and outlet, denoted as the tunnel Inlet (h_{in}) / tunnel Outlet (h_{out}) as demonstrated in Figure 6. This ratio is studied to assess the impact of channel flow on the overall aerodynamic behavior of the system.

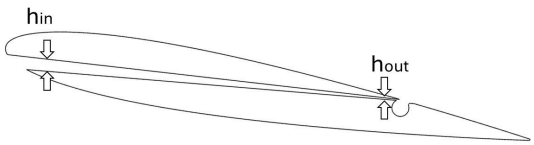

Figure 6: NACA0012 with the passive blowing tunnel: h_{in} represents the tunnel inlet; h_{out} represents the tunnel outlet: Upper side is suction surface and bottom side is pressure surface

B. Active vs. Passive blowing

Both active and passive flow control methods share the common objective of increasing the blowing effect within the cavity to amplify the suction effect along the trailing edge of the suction surface after airflow exits the TVC. However, these methods achieve this goal through fundamentally different approaches.

In the active flow control case, additional energy input is required to create an external blowing effect inside the cavity. This is achieved by applying a blowing power, which is measured based on the mass-flow rate as the energy input parameter. A constant length ratio of the blowing slot to the TVC diameter is incorporated along the edge of the cavity, and the blowing power is varied by adjusting the mass-flow rate. In this study, the mass-flow rate is represented by V_{in}/V_{∞}, which V_{in} refers to the velocity exiting from the blowing slot and V_{∞} refers to the velocity imposed at the inlet.

In contrast, the passive flow control case does not require additional energy input. Instead, a geometrical modification is introduced to generate a free-blowing effect. A blowing tunnel is designed, extending from the stagnation point of the airfoil to the TVC. The high-pressure region at the stagnation point provides the necessary blowing energy directly into the cavity. The ratio $h_{\text{in}}/h_{\text{out}}$ is varied to examine the effect of the strength of the blowing mechanism, with h_{out} and $\text{TVC}_{\text{diameter}}$ kept constant. The ratio between h_{in} and h_{out} with $\text{TVC}_{\text{diameter}}$ is shown in Table I. An increase in the $h_{\text{in}}/h_{\text{out}}$ ratio corresponds to a larger tunnel entrance at the stagnation point, allowing a greater volume of high-pressure air to enter the cavity. This, in turn, enhances the observed blowing effect.

$\frac{h_{\text{in}}}{h_{\text{out}}}$ [−]	$\frac{h_{\text{out}}}{\text{TVC}_{\text{Diameter}}}$ [−]	$\frac{h_{\text{in}}}{\text{TVC}_{\text{Diameter}}}$ [−]
NACA0012 Case		
1.0	0.1875	0.1875
2.0	0.1875	0.375
3.0	0.1875	0.5625
4.0	0.1875	0.75
5.0	0.1875	0.9375
6.0	0.1875	1.125
7.0	0.1875	1.3125
Three-element Airfoils Case		
1.0	0.18	0.18
2.0	0.18	0.36
3.0	0.18	0.54
4.0	0.18	0.72
5.0	0.18	0.90
6.0	0.18	1.08
7.0	0.18	1.26

Table I: Dimensions of Passive Blowing Tunnel of NACA0012 and Three-element Airfoils

C. Grid Settings

The computational grids for the NACA0012 airfoil and the front airfoils were generated using Fidelity Pointwise. Quadrilateral elements were used in the inflation layer near wall boundaries using a wall-resolved approach. A $y^+ = 1$ was set, with a growth rate of 1.2 and sufficient cells to cover the entire boundary layer. The farfield was filled with a quad-dominant advancing front approach, applying local refinement around the airfoil geometries. This grid setup was applied uniformly across all simulations to ensure consistency and accuracy in the boundary layer resolution.

D. CFD Setup

All simulations were performed using an incompressible solver setup, solving the Reynolds-averaged Navier-Stokes (RANS) equations. SIMPLE algorithm is employed for coupling pressure and velocity and the k-ω SST turbulence model to capture turbulence. The simulations were deemed converge after the average lift and drag coefficient did not change by more than 0.1% over an averaging window size of 50.

E. Boundary condition

The inlet boundary condition was specified for the simulations as a velocity inlet. In the case of the NACA0012 airfoil, the freestream Reynolds number was set to 6×10^6, while for the front wing airfoils, it was set to 1.5×10^6. In both cases, the turbulence intensity was defined as 5%, and the turbulent viscosity ratio was set to 10. The outlet boundary condition was defined as a pressure outlet with a gauge pressure of 0 Pa.

For the NACA0012 airfoil, both the top and bottom boundaries were specified with a zero-shear stress condition. For the three element airfoil case, the top boundary maintained the same zero-shear stress condition, but a moving ground was utilised, where the moving ground and inlet velocity were matched.

The airfoil body and the front airfoils were assigned a no-slip boundary condition to accurately capture the viscous effects at the surface. Additionally, the slot was designated as a mass flow inlet.

IV. RESULTS AND DISCUSSION

A. Validation

N_{cells}	C_L	r	GCI	$GCI_{\text{asymptotic}}$	p	$C_{L_{\text{extrapolated}}}$
213189	1.0021e+00	1.50	0.09%			
97680	1.0028e+00	1.50	0.18%	1.043	1.83	1.00
43163	1.0012e+00	-	-			
N_{cells}	C_D	r	GCI	$GCI_{\text{asymptotic}}$	p	$C_{D_{\text{extrapolated}}}$
213189	1.8036e-02	1.50	0.01%			
97680	1.8040e-02	1.50	0.03%	1.025	4.66	1.80e-02
43163	1.8013e-02	-	-			

Table II: Grid convergence study of C_L and C_D over 3 grids for NACA0012

N_{cells}	C_L	r	GCI	$GCI_{\text{asymptotic}}$	p	$C_{L_{\text{extrapolated}}}$
165846	-1.247e+00	1.50	0.51%			
73499	-1.251e+00	1.48	0.86%	0.971	1.23	-1.24e+00
33463	-1.245e+00	-	-			
N_{cells}	C_D	r	GCI	$GCI_{\text{asymptotic}}$	p	$C_{D_{\text{extrapolated}}}$
165846	2.267e-02	1.50	0.40%			
73499	2.245e-02	1.48	1.69%	0.966	3.49	2.27e-02
33463	2.335e-02	-	-			

Table III: Grid convergence study of C_L and C_D over 3 grids for the three-element airfoils

A grid convergence study was conducted for the NACA0012 airfoil and the three element airfoils to evaluate the lift coefficient (C_L) and drag coefficient (C_D) across coarse, medium, and fine grid. The results are shown in Tables II–III. The extrapolated values of C_L and C_D are denoted by $C_{L,\text{extrapolated}}$ and $C_{D,\text{extrapolated}}$. The parameter N_{cells} represents the number of grid elements, while r is the grid refinement ratio between two successive grids. The grid convergence index (GCI) is calculated as a percentage to quantify the uncertainty associated with the grid resolution. The asymptotic value of the GCI, denoted as $GCI_{\text{asymptotic}}$, is used to assess the proximity of the solution to grid independence. The order of accuracy, p, achieved in the simulations was also determined. The fine grids were selected for further analysis based on the grid convergence study results.

The lift coefficient (C_L) and drag coefficient (C_D) of the clean NACA 0012 airfoil without a Trapped Vortex Cavity (TVC) were obtained from CFD simulations for angles of incidence ranging from 0° to 20°. These results were compared with the experimental data from Ladson [20] at a Reynolds number of $Re = 6 \times 10^6$ to validate the CFD model, as shown in Figure 7. In

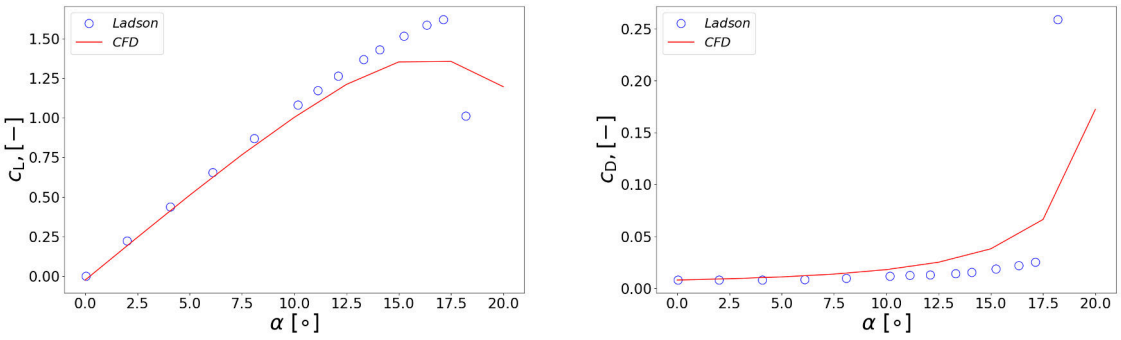

(a) c_L (b) c_D

Figure 7: Simulation validation with Experimental result by Ladson [20], $\alpha[^\circ]$ represents angle of attack, $c_L[-]$ represents the Lift coefficient, and $c_D[-]$ represents the Drag coefficient

Ladson's experiments, a trip wire was placed near the leading edge of the airfoil to induce a fully turbulent boundary layer, ensuring a fully turbulent flow around the airfoil. This approach, including the same inlet conditions, was adopted in this study to ensure consistency with the experimental setup and to align with the turbulence modeling methodology.

Both C_L and C_D values from the CFD simulations showed good agreement with the experimental data for angles of incidence below the stall angle. Although the CFD simulations predict slightly higher C_D values than the experimental results, the overall trend is well captured, attesting to a good qualitative match with the experimental data.

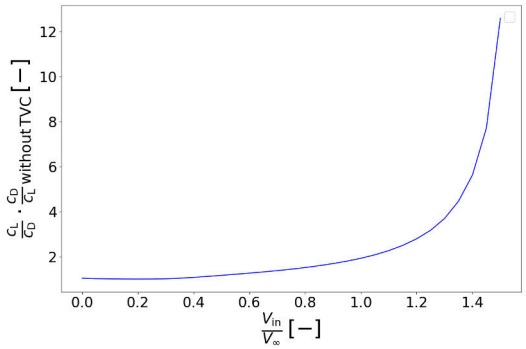

Figure 8: NACA0012 attached with TVC with mass-flow rate anachored inside the cavity: $V_{in}/V_\infty[-]$ represents the mass-flow rate in term of velocity entering into the cavity versus free-stream velocity; $c_L/c_D[-]$ represent Lift coefficient versus Drag coefficient

B. 2D NACA0012

1. *Active Aerodynamics Case*

A parametric study presented in Figure 8 was conducted to evaluate the effectiveness of the *TVC* system under varying mass-flow rates, with a fixed TVC diameter equals to 0.29 $TVC_{diameter}/Airfoil_{thickness}[-]$. The mass-flow rate is calculated from Eq. (1), where V_{in} is the velocity exiting from the blowing slot, as mentioned in Figure 5, and V_∞ is the velocity imposed at the inlet. The ratio V_{in}/V_∞ serves as a dimensionless measurement of the mass-flow rate, which is used to evaluate the effect of the blowing slot on the C_L/C_D. The C_L/C_D of the NACA0012 airfoil equipped with the TVC system is compared to the C_L/C_D of the original NACA0012 airfoil without the TVC system to facilitate a dimensionless comparison. For this purpose, the ratio C_L/C_D normalized by $C_L/C_{D\text{without TVC}}$ is presented on the y-axis. A reference value of 1 is used to indicate the condition where the performance of the airfoil with the TVC system is equivalent to that of the original airfoil without the system under the same circumstances.

The result indicates that the introduction of mass flow into the cavity leads to an improvement in the C_L/C_D. Even at zero mass flow, the C_L/C_D ratio of the airfoil with TVC is 5.1% higher than that of a clean airfoil. As the mass-flow rate increases beyond $0.4\,V_{\text{in}}/V_\infty$, the C_L/C_D ratio rises steeply, reaching a maximum value at $1.5\,V_{\text{in}}/V_\infty$. This represents a 12.6-fold improvement over the clean airfoil with TVC.

However, when V_{in}/V_∞ exceeds 1.5, the drag value

drops to nearly zero, and transitions into thrust at a ratio of 1.6. At this point, the original TVC functionality is essentially lost, as the system begins to behave more like an air-jet, deviating from the core focus of the research. Therefore, in the case of the NACA0012 airfoil, the mass-flow rate has been limited to values corresponding to $V_{\text{in}}/V_{\infty} \leq 1.5$, ensuring that the investigation remains aligned with the intended objectives of the study.

The significant increase in the C_L/C_D can be attributed to the enhancement of vortex strength as the mass-flow rate increases. The velocity of the airflow exiting the slot not only helps trap the vortex but also drives some of the airflow divided at the stagnation point into the cavity, thereby strengthening the vortex. The intensified vortex accelerates the flow, leaving the cavity and producing a suction peak near the exit of the TVC. The accelerated flow leads to a reduction in static pressure along the suction surface, which contributes to an increase in downforce.

Additionally, the accelerated flow near the trailing edge of the TVC promotes flow reattachment, preventing flow separation and significantly reducing drag. Consequently, as the mass-flow rate increases, a larger suction peak forms near the TVC edge, accelerating the airflow over the airfoil and further improving the C_L/C_D ratio. With sufficient mass-flow input, the C_L/C_D ratio can exceed that of a clean airfoil by more than 12.6 times, offering substantial aerodynamic benefits.

While an improvement in C_L/C_D has been observed with the active aerodynamic system, this improvement comes at the cost of external energy input required to pump fluid away from the boundary layer and energize the flow. The system depends on continuous energy supplied through the blowing slot to maintain vortex strength, as demonstrated by the mass-flow rate equation (Eq. 1). However, the actual energy cost of operating the active system needs to be further investigated to evaluate its overall efficiency for practical applications.

To address this potential limitation, a passive aerodynamic case has been introduced as an alternative method. Unlike the active system, the passive approach relies solely on geometrical modifications to enhance C_L/C_D without requiring external energy inputs. This method explores whether changes in geometry, represented by the ratio $h_{\text{in}}/h_{\text{out}}[-]$, can achieve similar aerodynamic performance while minimizing the need for mass-flow rates and energy input.

2. *Passive Aerodynamics Case*

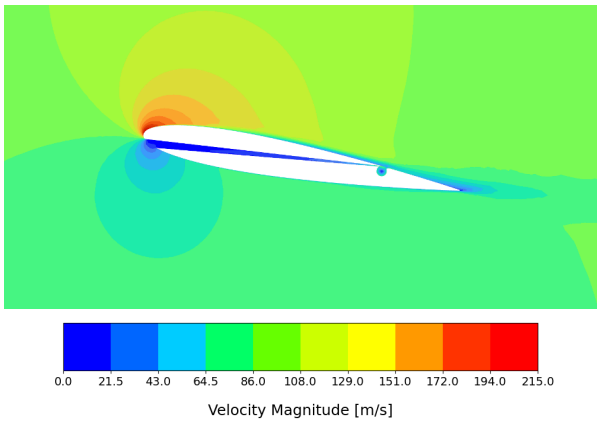

Figure 9: Velocity contour of NACA0012 attached with trapped vortex cavity connected with passive blowing tunnel at its optimal ratio of 4. The color bar represents the velocity magnitude.

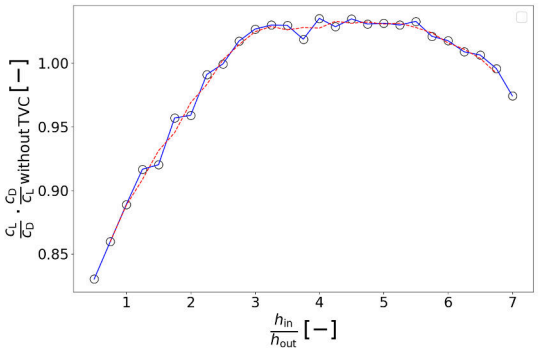

Figure 10: NACA0012 attached with TVC connected to passive blowing tunnel: $h_{in}/h_{out}[-]$ represents the length ratio between the channel inlet and channel outlet; $c_L/c_D[-]$ represent Lift coefficient versus Drag coefficient: The blue solid line represents results obtained from CFD while the red dashed line represents window-averaged results.

In the passive configuration of the NACA0012 airfoil, the tunnel was created, as illustrated in Figure 6. The tunnel geometry features a varying h_{in}/h_{out} in the range of $0.5 \leq h_{in}/h_{out} \leq 7$. The velocity contour around the airfoil is shown in Figure 9, and the C_L/C_D performance is presented in Figure 10.

Based on Figure 10, a steadily increasing trend of C_L/C_D is observed as the h_{in}/h_{out} increases. Initially, at lower ratios, the performance of the airfoil equipped

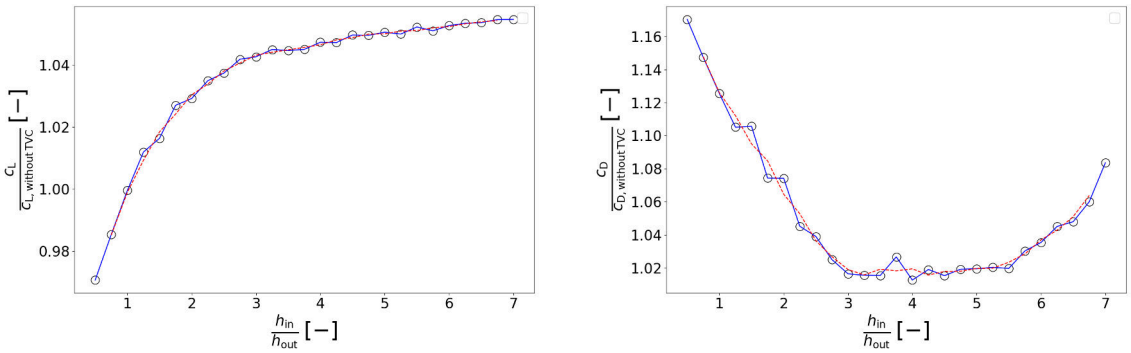

(a) c_L (b) c_D

Figure 11: NACA0012 attached with TVC connected to passive blowing tunnel: $h_{in}/h_{out}[-]$ represents the length ratio between the channel inlet and channel outlet; $c_L[-]$ represents Lift coefficient and $c_D[-]$ represents Drag coefficient.The blue solid line represents results obtained from CFD while the red dashed line represents window-averaged results.

with the channel and TVC is worse than that of the clean airfoil. However, once the h_{in}/h_{out} exceeds 2.5, the performance of the channel-equipped airfoil begins to surpass that of the clean airfoil.

The maximum improvement in C_L/C_D occurs at an h_{in}/h_{out} of 4, where a 3.52% increase in C_L/C_D is recorded compared to the clean airfoil. Beyond this point, however, the performance begins to decline. When the h_{in}/h_{out} reaches 6.5, the performance drops below that of the original clean airfoil.

Compared to a clean airfoil, the C_L of the channel-equipped TVC airfoil revealed in Figure 11, was investigated to understand better the aerodynamic principles of the TVC system linked with the channel. The results show that C_L increases rapidly within the h_{in}/h_{out} range of 1 to 4, where a maximum enhancement of 4.9% is recorded compared with the clean airfoil. Beyond a ratio of 4, the lift coefficient continues to increase but at a more gradual rate, reaching a 5.7% improvement at a ratio of 7.

Between the ratios of 1 and 4, the sharp increase in lift can be attributed to the increased mass-flow rate through the channel into the TVC cavity. As the channel inlet size increases, more high-pressure air from the stagnation point flows into the channel. This larger mass-flow rate, achieved without any external power input, accelerates as it moves through the channel, particularly near the outlet linked to the TVC. The accelerated flow creates a higher suction peak near the TVC edge and lowers the static pressure along the suction side of the airfoil.

This accelerated flow also enhances the vortex strength in the TVC, which plays a crucial role in trapping the vortex within the cavity. The stronger vortex further reduces pressure on the suction surface, thereby increasing lift.

However, beyond a ratio of 4, the increase in C_L becomes more gradual. This suggests that the incremental benefits of increasing the inlet size diminish, indicating that the channel-TVC system is reaching a saturation point. At this stage, the ability of the TVC to trap and maintain the vortex by relying solely on the passive mass-flow from the channel becomes limited, resulting in a performance plateau for this passive aerodynamic approach.

At an inlet/outlet ratio of 4, the sum of the drag contributions from the internal channel and the outer airfoil profile reaches its minimum value. The minimum C_D occurs alongside the rapid increase in the C_L, resulting in the highest C_L/C_D ratio among all the studied cases. Therefore, the h_{in}/h_{out} of 4 represents the optimal point where the aerodynamic performance, as measured by C_L/C_D, is maximized due to the balance between minimized drag and maximized lift.

The velocity contours of the NACA0012 airfoil's leading and trailing edges, with varying $h_{\text{in}}/h_{\text{out}}$ ratios, are illustrated in Figure 12 and Figure 13 to help visualize the performance trends as the parameters change. Figure 13 shows an enhancement in vortex strength when $h_{\text{in}}/h_{\text{out}}$ increases from 1 to 4. The increased vortex strength in the ratio of 4 leads to a higher ejected flow from the cavity, resulting in a smaller wake region than the $h_{\text{in}}/h_{\text{out}} = 1$ case. The

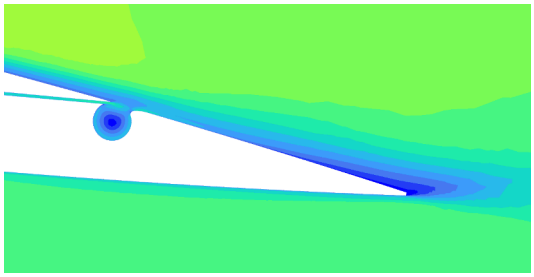

(a) $h_{in}/h_{out} = 1.0$

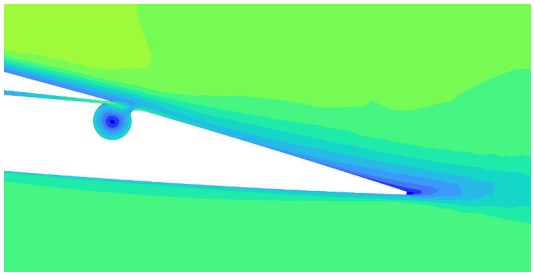

(b) $h_{in}/h_{out} = 2.5$

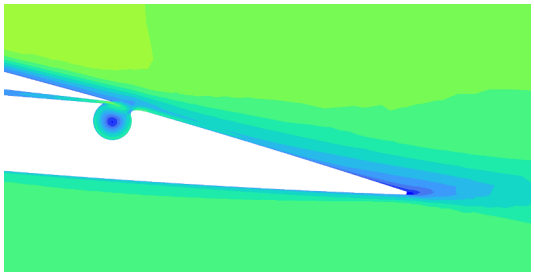

(c) $h_{in}/h_{out} = 4.0$

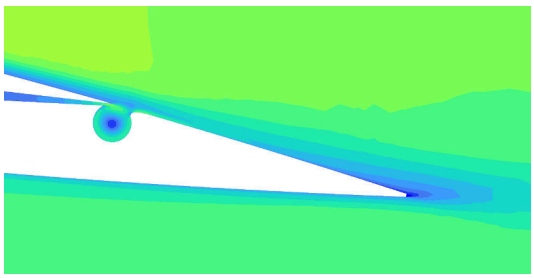

(d) $h_{in}/h_{out} = 7.0$

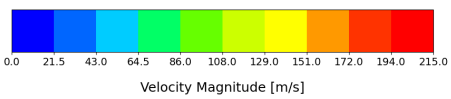

Figure 12: Velocity contours of the NACA0012 trailing edge at h_{in}/h_{out} ratios of 1.0, 2.5, 4.0, and 7.0. The color bar represents the velocity magnitude.

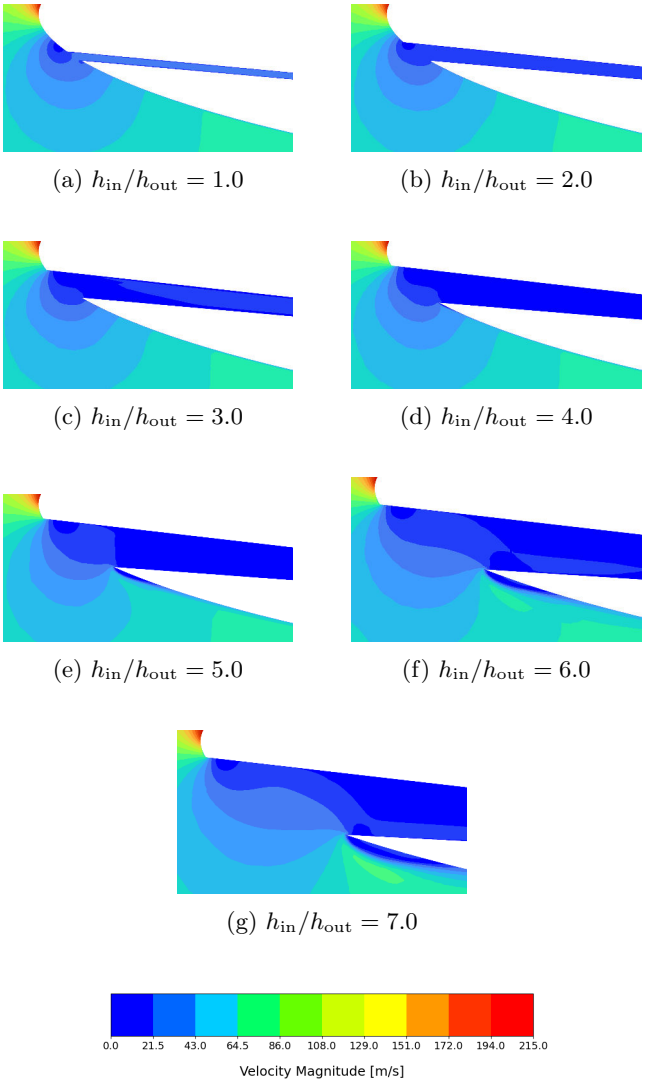

(a) $h_{in}/h_{out} = 1.0$

(b) $h_{in}/h_{out} = 2.0$

(c) $h_{in}/h_{out} = 3.0$

(d) $h_{in}/h_{out} = 4.0$

(e) $h_{in}/h_{out} = 5.0$

(f) $h_{in}/h_{out} = 6.0$

(g) $h_{in}/h_{out} = 7.0$

Figure 13: Velocity contours of the NACA0012 leading edge at h_{in}/h_{out} ratios ranging from 1.0 to 7.0. The color bar represents the velocity magnitude.

difference explains the rapid increase in C_L/C_D, as shown in Figure 10. However, when the ratio is below 2.5, despite a continuous reduction in the wake region with increasing h_{in}/h_{out}, the vortex strength remains insufficient, and the C_L/C_D is worse than that of the clean airfoil.

On the other hand, when the h_{in}/h_{out} ratio exceeds 4, only marginal changes in vortex strength inside the cavity are observed. The wake region size remains almost the same even as the ratio increases to 7. The similar size suggests that the tunnel reaches a saturation point, which correlates with the marginal improvement in C_L after an h_{in}/h_{out} ratio of 4, as shown in Figure 11.

Figure 13 further explains the performance reduction after a $h_{\text{in}}/h_{\text{out}}$ ratio of 4. A small recirculation region forms at the pressure surface near the tunnel entrance at the leading edge when the ratio exceeds 4. This recirculation area delays the splitting air flow to attach to the pressure surface of the airfoil, thus increasing drag, as shown in Figure 11. Combined with the marginal improvement in lift, this results in a reduction in C_L/C_D performance.

C. 2D Front Wing

1. *Active Aerodynamics Case - TVC at slat, flap and different chord length of mid airfoils*

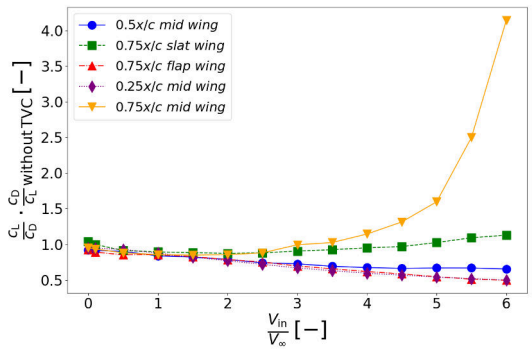

Figure 14: Three-element airfoils performance of TVC with located in different chord locations on mid airfoil, slat airfoil and flap airfoil: $V_{in}/V_\infty[-]$ represents the mass-flow rate in term of velocity entering into the cavity versus free-stream velocity; $c_L/c_D[-]$ represent Lift coefficient versus Drag coefficient

After results on the NACA 0012 airfoil suggest that a performance increase can be expected even for the passive aerodynamic case, the TVC was applied to the three element airfoil wing as shown in Figure 2. The results of the parametric studies are given in Figure 14, where the radius of the TVC was kept constant. The TVC was tested at different positions for each element of the three-element airfoil. Specifically, the TVC was positioned at $x/c = 0.75$ for the slat, at $x/c = 0.75$ for the flap, and at $x/c = 0.25$, $x/c = 0.50$, and $x/c = 0.75$ for the mid airfoil in separate cases. The findings indicate that, among these configurations, placing the TVC at the trailing edge of the mid airfoil ($x/c = 0.75$) yielded the highest C_L/C_D, achieving a value approximately four times greater than that of the original three-element airfoil without TVC at a mass-flow rate ratio of 6 V_{in}/V_∞.

The superior performance of the mid-airfoil TVC can be attributed to its ability to enhance flow control capabilities and delay flow separation more effectively than the slat and flap configurations. Increasing the mass flow rate through the TVC resulted in a reduction of static pressure on the suction surface of the mid airfoil, which contributed to increased downforce. Additionally, the proximity to the ground restricted airflow beneath the airfoil, which promoted stronger flow attachment in conjunction with the mid-airfoil's negative camber. The application of blowing flow via the TVC further augmented the downforce, explaining the significantly higher C_L/C_D.

The increased aerodynamic efficiency of the mid airfoil, compared to the other elements, is also influenced by its central position within the three-element system, allowing for beneficial interactions with both the slat and the flap. By reducing pressure peaks and delaying boundary layer separation, the slat airfoil delivers a thinner boundary layer to the mid-airfoil's leading edge, enabling it to withstand stronger adverse pressure gradients [23]. This interaction mitigates drag increase and contributes to the overall improvement in C_L/C_D. Furthermore, the accelerated flow discharged from the TVC on the mid airfoil enhances the dumping effect on the flap, resulting in high-velocity, attached flow downstream. This interaction intensifies the downforce produced by the flap, further increasing the system's overall aerodynamic effectiveness.

In contrast, the placement of the TVC on the slat was found to be less effective in generating downforce, as shown in Figure 15. Although the TVC on the slat stabilized the flow and delayed separation on the mid airfoil, its impact on downforce was limited due to the slat's relatively flat geometry and lower camber, which restricted the acceleration of the flow beneath it. Additionally, the slat's position, being further upstream, limited its ability to directly energize the flow over the flap, resulting in a lower overall C_L/C_D compared to the mid airfoil configuration.

The application of the TVC to the flap produced substantial downforce comparable to that observed in the mid-airfoil configuration. However, this came at the cost of a significant drag increase, as shown in Figure 15, leading to the lowest C_L/C_D among the three configurations. The large flap deflection angle at the trailing edge, augmented by the TVC, energized the underbody flow, contributing to increased downforce. However, the high flap angle also induced a thicker boundary layer and less effective pressure recovery, which expanded the wake region and resulted in a

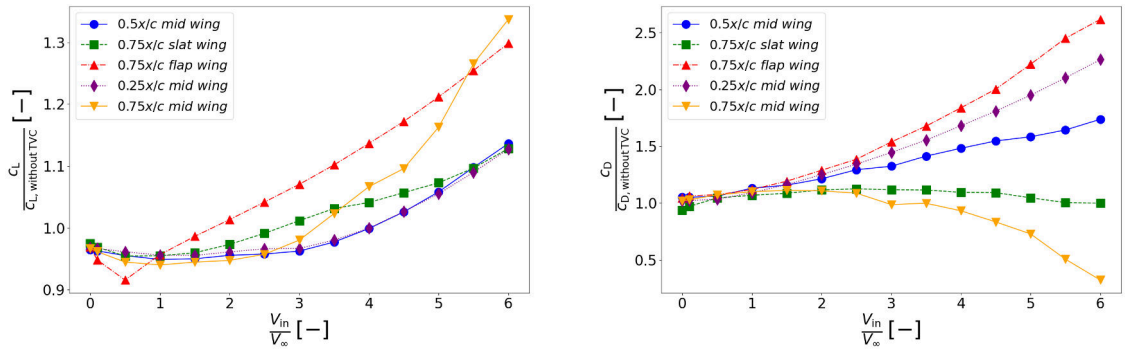

(a) c_L (b) c_D

Figure 15: Three-element airfoils performance of TVC with located in different chord locations on mid airfoil, slat airfoil and flap airfoil

significant drag penalty.

The performance differences between the TVC placements at $x/c = 0.25$, $x/c = 0.50$, and $x/c = 0.75$ along the mid are presented in Figure 14 as well. The results indicate that positioning the TVC at $x/c = 0.25$ and $x/c = 0.50$ does not improve the aerodynamic performance of the airfoil. In fact, with increasing mass flow rate through the cavity, these configurations led to a deterioration in performance, consistent with the findings reported by [18], who investigated a similar setup on a single airfoil without an applied mass flow rate.

The negative impact of placing the TVC at the frontal and mid-chord locations can be attributed to the inability of the energized flow exiting the cavity to reattach to the trailing edge of the mid airfoil. As the mass flow rate inside the cavity increases, the enhanced flow energy causes premature flow separation. This early separation leads to increased drag as the flow fails to maintain attachment over the entire surface of the mid-wing. Consequently, placing the TVC at these locations results in a reduction in overall aerodynamic efficiency.

Thus, it is evident that placing the TVC at the trailing edge of the mid airfoil leverages the beneficial effects of the energized flow without inducing early separation, leading to a marked improvement in performance.

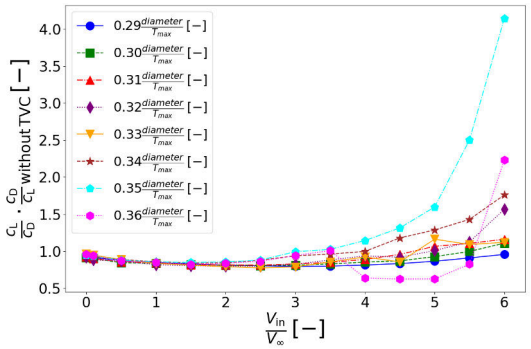

Figure 16: Comparison of different diameters of TVC located in mid airfoil: $V_{in}/V_\infty[-]$ represents the mass-flow rate in term of velocity entering into the cavity versus free-stream velocity; $c_L/c_D[-]$ represent Lift coefficient versus Drag coefficient; $diameter/T_{max}[-]$ represent TVC diameter versus Mid airfoil thickness

2. *Active Aerodynamics Case - TVC with diameters variation*

Parametric studies were conducted to evaluate the aerodynamic performance of the front airfoils with varying TVC diameter ratios, defined as $D/T_{\max}$, where D is the diameter of the TVC and $T_{\max}$ is the maximum thickness of the mid airfoil. The results, shown in Figure 16, reveal that for diameter ratios ranging from 0.29 to 0.35, the C_L/C_D ratio increases as the mass-flow rate increased. Larger $D/T_{\max}$ ratios contribute to higher C_L/C_D values, with the maximum performance observed at a diameter ratio of 0.35. At this ratio, the C_L/C_D reaches up to four times that of

the original clean three-element airfoils at a mass-flow rate of 6 V_{in}/V_{∞}.

However, the performance of the 0.36 diameter ratio experiences a noticeable reduction compared to the 0.35 ratio despite still achieving the second-highest C_L/C_D at 6 V_{in}/V_{∞}, approximately twice the value of the clean airfoil. This performance drop is more pronounced at lower mass-flow rates than higher, where the 0.36 diameter ratio records a significant reduction in C_L/C_D. In contrast, smaller diameter ratios ($D/T_{\max} < 0.35$) show proportional performance improvements with increasing mass-flow rates, although their rate of increase is slower compared to the 0.35 ratio.

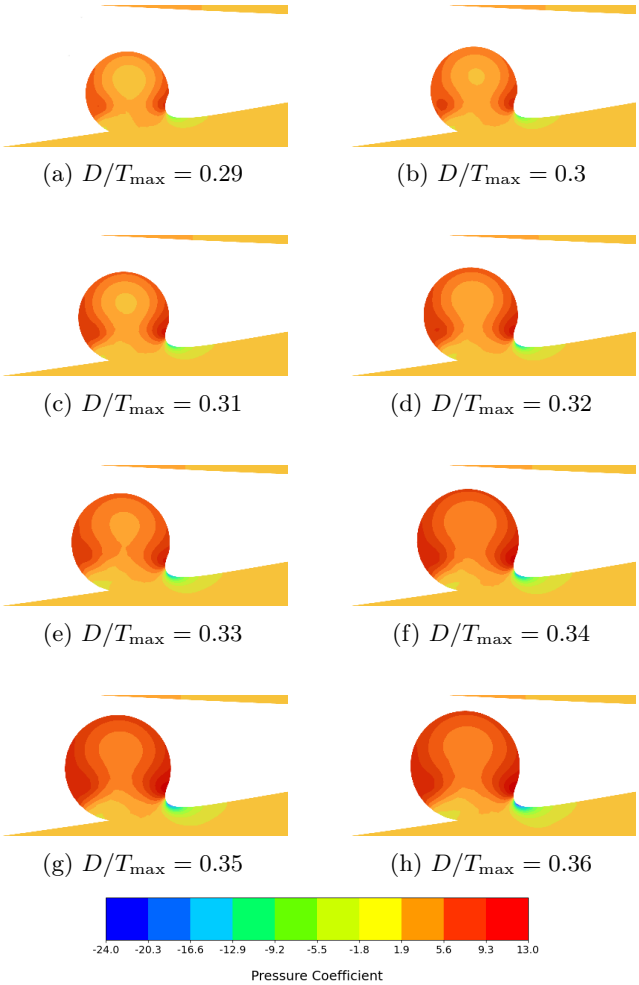

(a) $D/T_{\max} = 0.29$ (b) $D/T_{\max} = 0.3$

(c) $D/T_{\max} = 0.31$ (d) $D/T_{\max} = 0.32$

(e) $D/T_{\max} = 0.33$ (f) $D/T_{\max} = 0.34$

(g) $D/T_{\max} = 0.35$ (h) $D/T_{\max} = 0.36$

Figure 17: Pressure contours at different diameter-to-thickness ratios $D/T_{\max}$.

The pressure contours for each $D/T_{\max}$ ratio, presented in Figure 17, provide insights into the aerodynamic behavior of the TVC. Across all cases, a region of low static pressure consistently forms near the exit

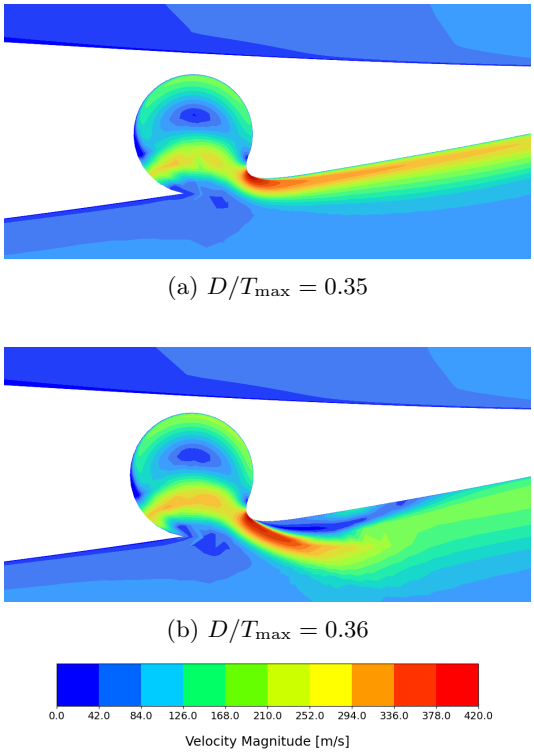

(a) $D/T_{\max} = 0.35$

(b) $D/T_{\max} = 0.36$

Figure 18: Velocity contours at 0.35 and 0.36 diameter-to-thickness ratios.

of the TVC. As the diameter of the cavity increases, the static pressure near the cavity's exit (adjacent to the stagnation point) further decreases. This suggests that for a given mass-flow rate, a larger TVC diameter creates a lower static pressure region near the cavity exit, which enhances the suction effect. This effect contributes to increased downforce, as the lower static pressure aids in maintaining flow attachment, thereby improving C_L/C_D.

The pressure contour analysis confirms that larger TVC diameters enhance the suction effect, which generates greater downforce and helps the flow reattach more effectively to the wing surface. This explains why increasing the diameter ratio up to 0.35 improves aerodynamic efficiency.

The velocity contours for the 0.35 and 0.36 diameter ratios, shown in Figure 18, explain the performance drop observed for the 0.36 diameter ratio. While the ejected flow in the 0.35 case smoothly reattaches to the trailing edge of the airfoil, the 0.36 diameter ratio generates a recirculation region near the cavity exit. This recirculation delays the flow reattachment to the airfoil, resulting in increased flow instability and separation. The delayed reattachment also enlarges the

wake region, thereby increasing pressure drag.

This increased drag, rather than a reduction in lift, explains the performance degradation for the 0.36 diameter ratio when the mass-flow rate increases. The larger recirculation bubble and delayed flow reattachment cause a significant drag penalty, which offsets the lift gains from the enhanced suction effect, thereby reducing the overall C_L/C_D performance.

3. *Passive Aerodynamics Case- Performance Comparsion between slat, mid flap airfoil*

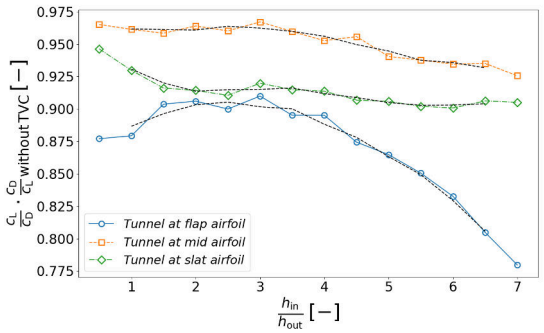

Figure 19: Three element airfoils attached with TVC connected to passive blowing tunnel respectively: $h_{in}/h_{out}[-]$ represents the length ratio between the tunnel inlet and tunnel outlet; $c_L/c_D[-]$ represent Lift coefficient versus Drag coefficient

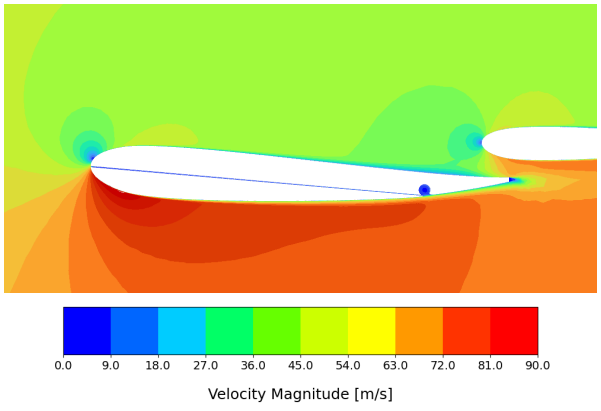

Figure 20: Velocity contour of slat attached with TVC connected to passive blowing tunnel at its optimal ratio of 0.5

Figure 19 shows the performance of the TVC with a passive blowing channel located in the slat. Initially, at $h_{in}/h_{out} = 0.5$, with its velocity contour shown in Figure 20, the C_L/C_D ratio reaches its peak, achieving approximately 0.95 times the value of the clean three-element airfoils. However, as the h_{in}/h_{out} ratio increases, the performance oscillates, with a gradual reduction in effectiveness. The oscillation suggests that while the passive blowing in the slat region shows some initial promise, it leads to unstable flow behavior as the ratio increases, decreasing the overall C_L/C_D ratio and indicating an unsatisfactory performance in this passive aerodynamic case.

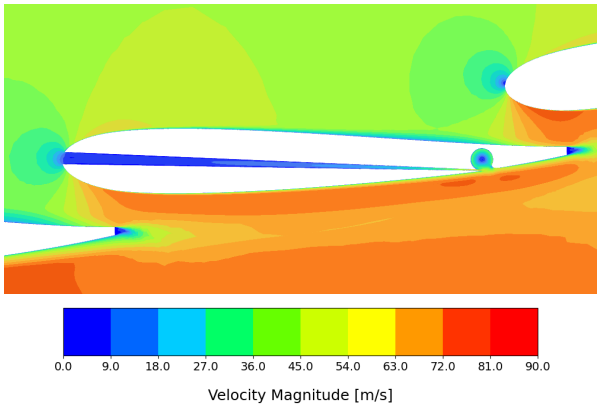

Figure 21: Velocity contour of mid attached with TVC connected to passive blowing tunnel at its optimal ratio of 3

Figure 19 illustrates the performance of the TVC with a passive blowing channel placed on the mid as well. The performance shows an oscillatory increase as the $h_{in}/h_{out}[-]$ ratio rises from 0.5 to 3. The C_L/C_D ratio continues to improve and reaches a maximum of 0.96 times the value of the clean three-element wing. The velocity contour of the optimal ratio of 3 is shown in Figure 21. Although this is slightly lower than the clean airfoils, the mid configuration performs better than the slat and flap setups. The oscillatory nature of the performance increase suggests that flow instabilities are present. However, the overall trend shows that the mid-airfoil configuration is better suited to passive blowing, as observed in the active aerodynamics cases.

The flap configuration, shown in Figure 19, follows a similar trend to the mid-wing. The C_L/C_D ratio oscillates and increases as the $h_{in}/h_{out}[-]$ ratio grows from 0.5 to 3. However, the maximum performance achieved here is around 0.91 times the value of the clean three-element airfoils, which is lower than the mid and slat configurations. The velocity contour in which the maximum C_L/C_D ratio is reached in the flap is shown in Figure 22. Beyond a ratio of 3, the performance

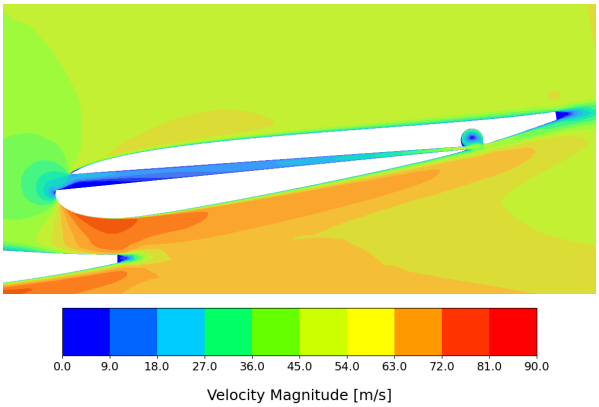

Figure 22: Velocity contour of flap attached with TVC connected to passive blowing tunnel at its optimal ratio of 3

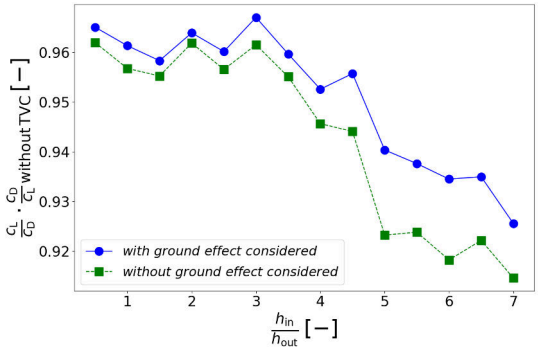

Figure 23: Comparsion of three-element airfoils with TVC and internal tunnel in mid with and without ground effect considered: $h_{in}/h_{out}[-]$ represents the length ratio between the tunnel inlet and tunnel outlet; $c_L/c_D[-]$ represent Lift coefficient versus Drag coefficient

begins to decline. Among the three configurations, the flap region shows the slightest improvement in C_L/C_D, indicating that the passive blowing channel is the least effective in this location.

The passive aerodynamic case involving the TVC and internal channels linking the slat, mid, and flap airfoils has yielded results that differ significantly from those previously observed in single-airfoil configurations. Two studies have been conducted to identify potential factors affecting the internal tunnel's performance in the three-element airfoils. In both cases, the TVC model with a passive blowing channel placed at the mid airfoil, demonstrating the best performance among the three-element airfoils, is used.

These studies intend to investigate the influence of ground proximity and three-element airfoil interactions on the internal tunnel's performance. The independent variables in these experiments are the presence of ground proximity and the interaction between the slat, mid, and flap airfoils, and the dependent variable is defined as the C_L/C_D performance of the three-element airfoils and the internal tunnel.

In the first study, the airfoil configuration is placed in free-stream conditions without the influence of ground proximity, consistent with the NACA0012 case. This setup allows for isolating the effects of the three-element airfoil interactions on the tunnel's performance. In the second study, ground proximity is maintained. However, the slat and flap airfoils are removed, focusing solely on the mid airfoil's tunnel and its performance in the absence of interactions with the other elements.

Figure 23 illustrates the C_L/C_D performance of the TVC with the passive blowing channel placed on the mid airfoil, both with and without ground effect. The results are compared with the C_L/C_D performance of the original three-element airfoil under the same ground effect and free-stream conditions. Both configurations exhibit a similar trend: the C_L/C_D ratio oscillates, rising steadily as the $h_{\text{in}}/h_{\text{out}}$ ratio increases from 1 to 3, reaching a maximum at 3, then rapidly decreasing continuously from 3 to 7. This behavior is consistent across both cases, as the same three-element airfoil configuration is used.

However, across all $h_{\text{in}}/h_{\text{out}}$ ratios, the C_L/C_D performance is worse in the absence of ground proximity than in the low ground clearance condition. The discrepancy between the two cases becomes more pronounced as the $h_{\text{in}}/h_{\text{out}}$ ratio increases. The finding suggests that ground proximity provides a positive aerodynamic effect on the tunnel's performance. As shown in Figure 24 of the pressure contours, the presence of ground effect results in a lower static pressure region forming between the mid airfoil and the ground, mainly due to the negative camber of the mid airfoil. This low-pressure region near the tunnel outlet enhances suction in the area, increasing the pressure differential between the tunnel inlet and outlet. Consequently, this leads to higher tunnel efficiency than the case without ground proximity. Therefore, ground proximity has a beneficial impact on the overall aerodynamic efficiency of the system.

Figure 25 presents the C_L/C_D performance of the internal tunnel in the mid airfoil configuration with

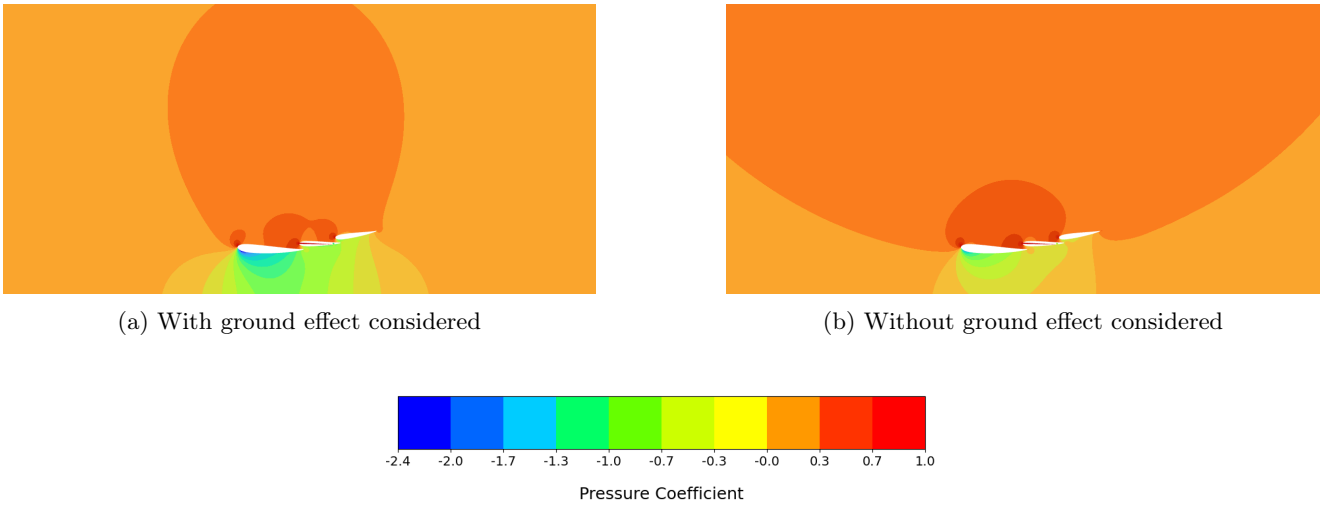

(a) With ground effect considered

(b) Without ground effect considered

Figure 24: Pressure contour of the three-element airfoils with TVC linked with the tunnel in mid airfoil. The color bar represents the pressure magnitude.

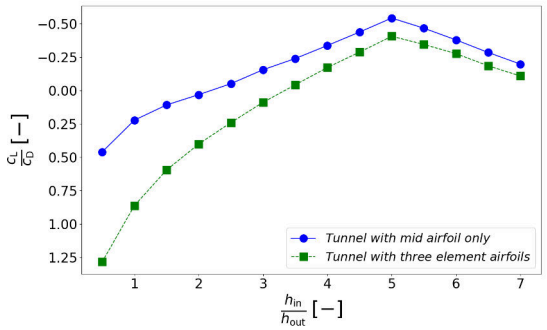

Figure 25: Comparison of tunnel performance for single mid airfoil and three-element airfoils: $h_{in}/h_{out}[-]$ represents the length ratio between the tunnel inlet and tunnel outlet; $c_L/c_D[-]$ represent Lift coefficient versus Drag coefficient

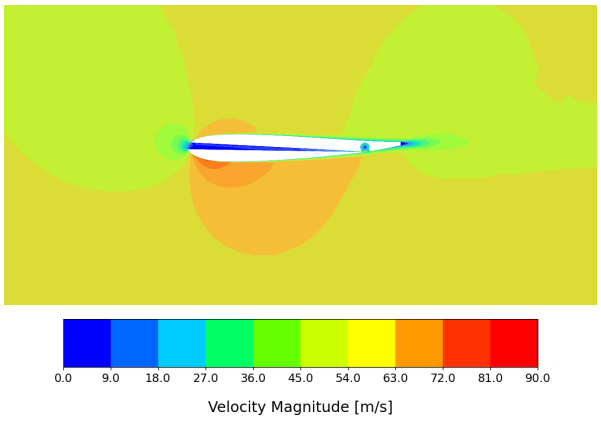

Figure 26: Velocity contour of single mid airfoil case

the velocity contour displayed in Figure 26, comparing the case where the slat and flap have been removed to the case where both the slat and flap are present. This plot focuses on the performance of the tunnel itself, and as such, the C_L/C_D performance is not normalized with $C_L/C_{D\text{without TVC}}$, since the original three-element airfoil does not include a tunnel, making such a comparison invalid. Instead, the purpose of this plot is to reveal the independent aerodynamic performance of the tunnel in each configuration. The plot reveals that both configurations follow a similar trend with varying $h_{\text{in}}/h_{\text{out}}$ ratios. C_L/C_D reaches its maximum at a ratio of 5, followed by a steady decrease beyond this ratio. However, at each $h_{\text{in}}/h_{\text{out}}$ ratio, the tunnel in the mid-airfoil-only configuration consistently generates a higher C_L/C_D compared to the tunnel with the three-element airfoils.

Further analysis of the C_L and C_D for the performance of the tunnel, as shown in Figure 27, shows that the mid-airfoil-only configuration produces a higher downforce (C_L) than the three-element airfoil configuration. Interestingly, despite the increase in downforce, the drag coefficient (C_D) remains nearly the same for both configurations. The result suggests that the presence of the slat and flap may negatively impact the tunnel's efficiency, as their removal improves the tunnel's ability to generate downforce without increasing drag.

The reduction in tunnel efficiency when the slat and flap are present can be attributed to the flow interaction between the slat airfoil and the mid airfoil. The flow leaving the pressure surface of the slat is redirected

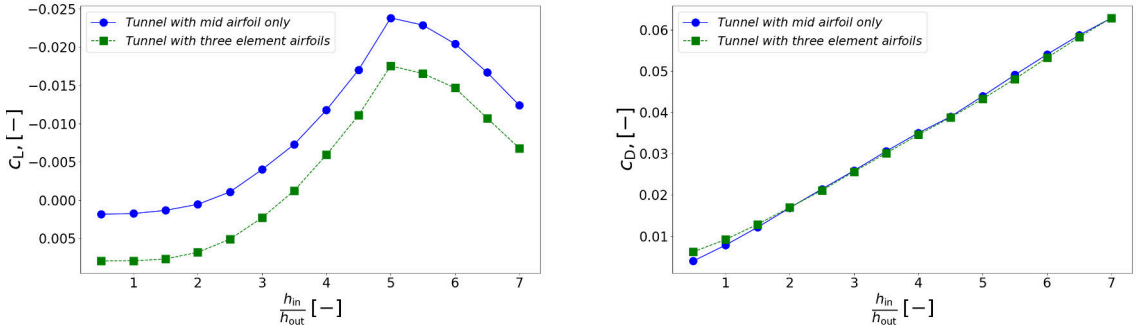

(a) c_L (b) c_D

Figure 27: Comparison of tunnel performance for single mid airfoil and three-element airfoils: $h_{in}/h_{out}[-]$ represents the length ratio between the tunnel inlet and tunnel outlet; $c_L/c_D[-]$ represent Lift coefficient versus Drag coefficient

towards the outer regions of the mid airfoil, and part of this flow is deflected towards the suction surface of the mid airfoil, altering the pressure distribution around it. While the three-element airfoil is designed to optimize and accelerate flow over the airfoil system, it inadvertently creates a boundary blockage effect near the tunnel entrance. This blockage restricts smooth airflow into the tunnel, reducing its overall efficiency.

In contrast, in the single mid airfoil case, the flow approaching the tunnel entrance is less disturbed and more aligned with the free-stream velocity direction. This results in a more streamlined flow into the internal tunnel, improving flow alignment at the tunnel entrance. The improved flow conditions contribute to higher tunnel efficiency, increasing downforce without any associated drag penalties.

Therefore, while the three-element airfoil is intended to improve overall aerodynamic performance, the interaction between the slat and mid airfoil creates adverse flow conditions at the tunnel entrance, reducing the effectiveness of the internal tunnel compared to the single mid airfoil configuration. The absence of the slat and flap allows for more favorable flow conditions, thereby improving the tunnel's performance.

Several alternative designs were explored to address these challenges, as presented in Figure 28, with the primary objective of providing more consistent airflow to the TVC. These designs were intended to minimize the unsteady flow interactions associated with the slat and flap regions by focusing on the mid location, where the flow is relatively more stable. Despite these efforts, all alternative configurations resulted in a lower C_L/C_D ratio than the original airfoil, suggesting that significant barriers exist to the successful implementation of a passive blowing channel in inverted three-element airfoils.

It is therefore concluded that, while the mid airfoil offers a more stable flow environment than the slat or flap regions, the inherent complexity of the flow generated, due to the interaction based on the three-element airfoils configuration, poses significant limitations on the effectiveness of the TVC in passive aerodynamics implementation.

V. CONCLUSIONS

Both active and passive aerodynamic approaches have been investigated through numerical methods for the NACA0012 airfoil and the cross-sectional area of the front wing of a Formula 1 car. The results indicate a significant improvement in the C_L/C_D ratio when active blowing flow is applied inside the TVC. This improvement is attributed to the high ejection flow from the TVC cavity, which generates a strong suction effect at the trailing edge. The enhanced suction effectively delays flow separation, resulting in higher aerodynamic efficiency compared to the original configurations.

The study of the Formula 1 front wing suggests that positioning the TVC at the trailing edge of the mid-airfoil yields the best performance in a three-element airfoil configuration. However, for the passive aerodynamics approach, while an improvement was observed in the NACA0012 airfoil, similar gains were not achieved for the front wing. This suggests that passive aerodynamics may be less effective for ground-effect

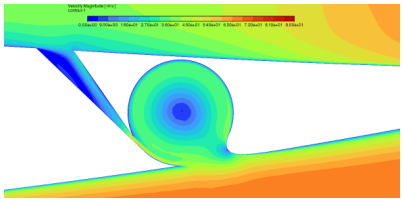

(a) $\frac{c_L}{c_D} \cdot \frac{c_D}{c_{L \text{ without TVC}}} = 0.955$

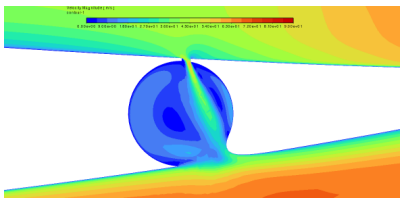

(b) $\frac{c_L}{c_D} \cdot \frac{c_D}{c_{L \text{ without TVC}}} = 0.916$

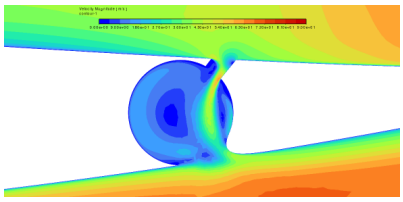

(c) $\frac{c_L}{c_D} \cdot \frac{c_D}{c_{L \text{ without TVC}}} = 0.899$

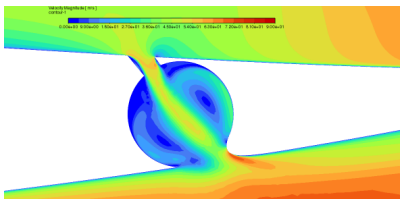

(d) $\frac{c_L}{c_D} \cdot \frac{c_D}{c_{L \text{ without TVC}}} = 0.880$

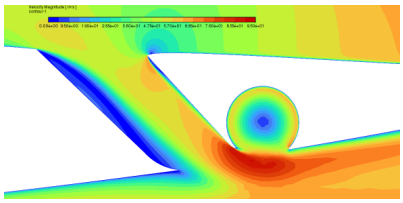

(e) $\frac{c_L}{c_D} \cdot \frac{c_D}{c_{L \text{ without TVC}}} = 0.823$

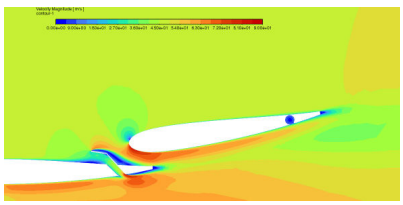

(f) $\frac{c_L}{c_D} \cdot \frac{c_D}{c_{L \text{ without TVC}}} = 0.603$

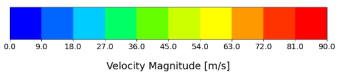

Figure 28: Alternative TVC and internal tunnel designs.

inverted three-element airfoils, where flow interactions are more complex.

For the active aerodynamic case, the TVC located at the trailing edge of the NACA0012 airfoil, combined with an optimized suction rate, recorded a 12.6-fold improvement, as observed in Figure 8, resulting in a maximum enhancement of 1160% in C_L/C_D compared to the original airfoil. For the three-element airfoil, with an optimal TVC position and an appropriate $D/T_{\max}$ ratio of 0.35, a 4-fold improvement was recorded, as shown in Figure 14. The best performance improvement was therefore 313% in C_L/C_D compared to the clean three-element airfoil configuration.

For passive aerodynamics, without additional power input, the NACA0012 achieved a maximum improvement of 3.52% in C_L/C_D. Despite optimizing the TVC position and using an appropriate $D/T_{\max}$ ratio, the maximum C_L/C_D for the three-element airfoil was only 96% of the original clean airfoil configuration.

The concept of the TVC can be extended to other critical aerodynamic components of a Formula 1 car, such as the rear diffuser. Integrating the TVC with active flow control could create a second pressure recovery region, amplifying the negative camber effect at the rear. This approach holds significant potential for balancing the front and rear aerodynamic forces, potentially improving the overall racing performance. Future research in this area, combined with the findings from the TVC application on the front wing, could provide valuable insights into optimizing the aerodynamic efficiency of Formula 1 cars.

DATA AVAILABILITY STATEMENT

All data supporting this study are included within this paper.

[1] Crowther, W.J., Jabbal, M., and Liddle, S.C., "Flow Control Fallacies: a Review of Common Pitfalls in Flow Control Research," Journal of Aerospace Engineering, Vol. 225, No. 1, pp. 1-11, 2011, DOI: 10.1243/09544100JAERO761.

[2] Katz, J., and Dykstra, L., "Effect of Wing/Body Interaction on the Aerodynamics of Two Generic Racing Cars" SAE Technical Paper 920349, 1992, DOI: 10.4271/920349.

[3] Garcia, D.L., and Katz, J., "Trapped Vortex in Ground Effect," AIAA Journal, Vol. 41, No. 4, pp. 674-678, 2003, DOI: 10.2514/2.1997.

[4] Katz, J., and Morey, F., "Aerodynamics of Large-Scale Vortex-Generator in Ground-Effect," Journal of Fluid Engineering, Vol. 130, No. 7, 2008, DOI: 10.1115/1.2948361.

[5] Kuya, Y., Takeda, K., and Zhang, X., "Flow Physics of a Race Car Wing With Vortex Generators in Ground Effect," Journal of Fluid Engineering, Vol. 131, No. 12, 2009, DOI: 10.1115/1.4000423.

[6] Basso, M., Cravero, C., and Marsano, D., "Aerodynamics Effect of the Gurney Flap on the Front Wing of a F1 Car and Flow Interactions with Car Components," Energies, Vol. 14, No. 8, pp. 2059, 2021, DOI: 10.3390/en14082059.

[7] Gudmundsson, S., Chapter 10 in "General Aviation Aircraft Design (Second Edition)," (Oxford, Butterworth-Heinemann, 2022).

[8] Ehirim, O.H., Knowles, K., and Saddington, A.J., "A Review of Ground-Effect Diffuser Aerodynamics," ASME Journal of Fluids Engineering, Vol. 141, Issue. 2, 020801, 2018, DOI: 10.1115/1.4040501.

[9] Ringleb, F.O., "Separation Control by Trapped Vortices," Boundary Layer and Flow Control, ed. G. V. Lachman, Pergamon Press, 1961.

[10] Kasper, W.A., "Some Ideas of Vortex Lift," Society of Automotive Engineers, Paper 750547, 1975.

[11] Kruppa, E.W., "A Wind Tunnel Investigation of the Kasper Vortex Concept," AIAA Paper 115704, 1977.

[12] Donelli, R.S., De Gregorio, F., and Iannelli, P., "Flow Separation Control by Trapped Vortex," 48th AIAA Aerospace Sciences Meeting, Paper 2010-1409, 2010, DOI: 10.2514/6.2010-1409.

[13] De Gregorio, F., and Fraioli, G., "Flow Control on a High Thickness Airfoil by Trapped Vortex Cavity," 14th International Symposium on Applications of Laser Techniques to Fluid Mechanics, 2008.

[14] Tutty, O.R., Buffoni, M., Kerminbekov, R., Donelli, R., De Gregorio, F., and Rogers, E., "Control of Flow with Trapped Vortices: Theory and Experiments," International Journal of Flow Control, Vol. 5, No. 2, pp. 89-109, 2013, DOI: 10.1260/1756-8250.5.2.89.

[15] Lasagna, D., Donelli, R., De Gregorio, F., and Iuso, G., "Effects of a Trapped Vortex Cell on a Thick Wing Airfoil," Experiments in Fluids, Vol. 51, No. 5, pp. 1369-1384, 2011, DOI: 10.1007/s00348-011-1160-9.

[16] Panigrahi, C., Chawla, R., and Nair, M.T., "Optimisation of Trapped Vortex Cavity for Airfoil Separation Control," Journal of Applied Fluid Mechanics, Vol. 15, No. 1, pp. 179-191, 2021, DOI: 10.47176/jafm.15.01.32684.

[17] Vuddagiri, A., Halder, P., Samad, A., and Chaudhuri, A., "Flow Analysis of Airfoil Having Different Cavities on its Suction Surface," Progress in Computational Fluid Dynamics, Vol. 16, No. 2, pp. 67, 2016, DOI: 10.1504/PCFD.2016.075151.

[18] Verma, A., Kulkarni, V., and Borah, B., "Cavity for Flow Control and Performance Improvement of Airfoil," presented at the ASME 2021 Gas Turbine India Conference, Online, Dec. 2-3, V001T05A004, 2021, DOI: 10.1115/GTINDIA2021-76415.

[19] Prince, S.A., Khodagolian, V., Singh, C., and Kokkalis, T., "Aerodynamics Stall Suppression on Airfoil Sections Using Passive Air-Jet Vortex Generators," AIAA Journal 47, no. 9 (2009): 1985-2270, doi:https://doi.org/10.2514/1.41986.

[20] Ladson, C.L., "NACA0012-Validation-Ladson-expdata," NASA Technical Memorandum NASA-TM-100526, 1988.

[21] "Suzuka F1 Circuit Layout and Records," F1 Fansite, https://www.f1-fansite.com/f1-circuits/suzuka-circuit/, accessed Nov. 2024.

[22] "Silverstone F1 Circuit Layout and Records," F1 Fansite, https://www.f1-fansite.com/f1-circuits/silverstone-circuit/, accessed Nov. 2024.

[23] Smith, A.M.O., "High Lift Aerodynamics," Journal of Aircraft, Vol. 12, No. 6, 1975.

On the application of trapped vortices in motorsport application for improved aerodynamic performance using passive and active flow controls

Ng, Ming Kin

2025-04-15

Ng MK, Teschner T-R. (2025) On the application of trapped vortices in motorsport application for improved aerodynamic performance using passive and active flow controls. SAE Technical Paper Series, April 2025, Article number 5029

https://doi.org/10.4271/2025-01-5029